

The dependence of the pairwise velocity dispersion on galaxy properties

Cheng Li,^{1,2,3*} Y. P. Jing,¹ Guinevere Kauffmann,³ Gerhard Börner,³
Simon D. M. White³ and F. Z. Cheng²

¹The Partner Group of MPI für Astrophysik, Shanghai Astronomical Observatory, Nandan Road 80, Shanghai 200030, China

²Center for Astrophysics, University of Science and Technology of China, Hefei, Anhui 230026, China

³Max-Planck-Institut für Astrophysik, Karl-Schwarzschild-Strasse 1, 85748 Garching, Germany

Accepted 2006 February 7. Received 2006 January 22; in original form 2005 September 30

ABSTRACT

We present measurements of the pairwise velocity dispersion (PVD) for different classes of galaxies in the Sloan Digital Sky Survey (SDSS). For a sample of about 200 000 galaxies with redshifts in the interval $0.01 < z < 0.3$, and r -band magnitudes $M_{0.1r}$ between -16 and -23 , we study the dependence of the PVD on galaxy properties such as luminosity, stellar mass (M_*), colour ($g - r$), 4000-Å break strength (D_{4000}), concentration index (C), and stellar surface mass density (μ_*). The luminosity dependence of the PVD is in good agreement with the results of Jing & Börner for the two-degree Field Galaxy Redshift Survey catalogue, once the photometric bandpass difference between the two surveys is taken into account. The value of σ_{12} measured at $k = 1 h \text{ Mpc}^{-1}$ decreases as a function of increasing galaxy luminosity for galaxies fainter than L^* , before increasing again for the most luminous galaxies in our sample. Each of the galaxy subsamples selected according to luminosity or stellar mass is divided into two further subsamples according to colour, D_{4000} , C and μ_* . We find that galaxies with redder colours and higher D_{4000} , C , and μ_* values have larger PVDs on all scales and at all luminosities/stellar masses. The dependence of the PVD on the parameters related to recent star formation (colour, D_{4000}) is stronger than on the parameters related to galaxy structure (C , μ_*), especially on small scales and for faint galaxies. The reddest galaxies and galaxies with high surface mass densities and intermediate concentrations have the highest pairwise peculiar velocities, that is, these move in the strongest gravitational fields. We conclude that the faint red population located in rich clusters is responsible for the high PVD values that are measured for low-luminosity galaxies on small scales.

Key words: galaxies: clusters: general – galaxies: distances and redshifts – cosmology: theory – dark matter – large-scale structure of Universe.

1 INTRODUCTION

The pairwise peculiar velocity dispersion (PVD) measures the relative motions of galaxies, and so reflects the action of the local gravitational fields. The PVD is thus an important quantity for probing the mean mass density Ω_0 of the Universe and the clustering power on small scales. It is widely used to constrain cosmogonic models and galaxy formation recipes (Davis et al. 1985). As a well-defined statistical quantity, the PVD can be estimated from redshift surveys, either by modelling redshift distortions in the two-point correlation function (2PCF), or by measuring the redshift-space power spectrum (Davis & Peebles 1983; Jing & Börner 2001b).

The first method relies on the fact that the peculiar motions of galaxies affect only their radial distances in redshift space. Thus

the information for peculiar velocities along the line of sight can be recovered by modelling the redshift-space 2PCF $\xi^{(s)}(r_p, \pi)$ as a convolution of the real-space 2PCF $\xi(r)$ with the distribution function of the pairwise velocity $f(v_{12})$:

$$\xi^{(s)}(r_p, \pi) = \int f(v_{12}) \xi \left(\sqrt{r_p^2 + (\pi - v_{12})^2} \right) dv_{12}, \quad (1)$$

where $v_{12} = v_{12}(r_p, \pi)$ is the pairwise peculiar velocity; r_p and π are the separations perpendicular and parallel to the line of sight. The real-space correlation function $\xi(r)$ is usually inferred from the projected 2PCF $w_p(r_p)$, which is a simple Abel transform of $\xi(r)$. However, the form of $f(v_{12})$ is not known from a rigorous theory. Based on the observational (Davis & Peebles 1983; Fisher et al. 1994) and theoretical considerations (e.g. Diaferio & Geller 1996;

*E-mail: leech@ustc.edu.cn

Sheth 1996), an exponential form is usually adopted:

$$f(v_{12}) = \frac{1}{\sqrt{2}\sigma_{12}} \exp\left(-\frac{\sqrt{2}}{\sigma_{12}} |v_{12} - \overline{v_{12}}|\right), \quad (2)$$

where $\overline{v_{12}}$ is the mean and σ_{12} is the dispersion of the one-dimensional peculiar velocities. Assuming an infall model for $\overline{v_{12}}(r)$, the PVD σ_{12} can then be estimated as a function of the projected separation r_p by comparing the observed $\xi^{(s)}(r_p, \pi)$ with the modelled one. The form of the infall model usually adopted is based on the self-similar solution and is a good approximation to the real infall pattern in the cold dark matter models with $\beta \equiv \sigma_8 \Omega_0^{0.6} \approx 0.5$ (Jing, Mo & Börner 1998, hereafter JMB98). Using this method and various redshift samples of galaxies, the measurement of PVD has been carried out by many authors (Davis & Peebles 1983; Mo, Jing & Börner 1993; Fisher et al. 1994; Zurek et al. 1994; Marzke et al. 1995; Somerville, Davis & Primack 1997). There have been significant variations in the results of these studies. In many cases, the measurement errors were underestimated and there were also problems due to ‘cosmic variance’ as a result of the limited volume contained in the early redshift surveys (Mo, Jing & Börner 1997). As a result, the early determinations are of limited power in constraining large-scale structure theories. The first accurate determination of the PVD ($\sigma_{12} = 570 \pm 80 \text{ km s}^{-1}$ at a projected separation $r_p = 1 h^{-1} \text{ Mpc}$) was presented by JMB98 using the Las Campanas Redshift Survey (LCRS), and has been verified by Zehavi et al. (2002) with the early data release of the Sloan Digital Sky Survey (SDSS) and by Hawkins et al. (2003) with the two-degree Field Galaxy Redshift Survey (2dFGRS). This value is substantially higher than the earlier results based on smaller surveys ($340 \pm 40 \text{ km s}^{-1}$) given by Davis & Peebles (1983). The large difference in these results is due to the fact that the value of the PVD is very sensitive to the presence (or absence) of rich clusters in a sample (Mo et al. 1993), and so a sample as large as LCRS is needed in order to give reliable estimates.

The PVD of galaxies can also be determined from the redshift-space power spectrum. Although the power spectrum is just the Fourier transform of the 2PCF, it is sometimes advantageous to work with the power spectrum instead of with the 2PCF. The advantage of using the redshift-space power spectrum to determine the PVD is that it is simple and accurate to model the infall effect (Jing & Börner 2004, hereafter JB04). It is also not necessary to assume a functional form for the real-space $P(k)$, as is usually required for the 2PCF. The relation between the power spectrum in redshift-space $P^{(s)}(k, \mu)$ and that in the real-space $P(k)$ can be written as (Peacock & Dodds 1994; Cole, Fisher & Weinberg 1995):

$$P^{(s)}(k, \mu) = P(k)(1 + \beta\mu^2)^2 D[k\mu\sigma_{12}(k)]. \quad (3)$$

Here k is the wavenumber, μ the cosine of the angle between the wavevector and the line of sight, and β the linear redshift-distortion parameter. The first multiplier after the power spectrum on the right-hand side of equation (3) is the Kaiser linear compression effect (Kaiser 1987), and the term D is the damping effect caused by the random motion of the galaxies. The damping function D , which should generally depend on k , μ and $\sigma_{12}(k)$, was found by Jing & Börner (2001a) to be a function of one variable $k\mu\sigma_{12}(k)$ only. They also found that, although the functional form of $D[k\mu\sigma_{12}(k)]$ depends on the cosmological model and bias recipes, for small k (large scales) where $D > 0.1$, $D[k\mu\sigma_{12}(k)]$ can be approximately expressed by the Lorentz form,

$$D(k\mu\sigma_{12}(k)) = \frac{1}{1 + (1/2)k^2\mu^2\sigma_{12}(k)^2}. \quad (4)$$

We will use equations (3) and (4) to derive σ_{12} and $P(k)$ from a measurement of the redshift-space power spectrum $P^{(s)}(k, \mu)$. However, when applying this method, there are a couple of important points that should be kept in mind. First, the Lorentz form is the Fourier transform of the exponential form of $f(v_{12})$ when σ_{12} is a constant and $\overline{v_{12}}$ is zero. This means that $\sigma_{12}(k)$ derived in the Fourier space is generally not the same as $\sigma_{12}(r)$ defined in the configuration space. Furthermore, even if σ_{12} is a constant, the redshift power spectrum of equation (3) may lead to an unphysical distribution of pairwise velocities in the configuration space when the infall is not zero (i.e. $\beta \neq 0$) (Scoccimarro 2004). Nevertheless, based on extensive tests of numerical simulations, Jing & Börner (2001a) demonstrated that, $\sigma_{12}(r)$ and $\sigma_{12}(k)$ have similar dependences on scale, and are different only by 15 per cent if $r = 1/k$ is used in the comparison. Therefore, the quantity $\sigma_{12}(k)$ can still be regarded as a good indicator for the PVD. Secondly, it is usually difficult to determine σ_{12} and β simultaneously, because there exists a strong degeneracy in determining these parameters (Peacock et al. 2001) from $P^{(s)}(k, \mu)$ at small scales. Moreover, there could be some luminosity dependence in β . JB04 investigated this by using the luminosity dependence of the bias parameter b given in (Norberg et al. 2002), and showed that their determinations of the PVD are robust to the reasonable changes of the β values. Thus a viable way to determine the PVD from $P^{(s)}(k, \mu)$ is to fix β at a reasonable estimate and then determine $P(k)$ and σ_{12} from the data. In this way, the real-space power spectrum $P(k)$ is mainly determined from $P^{(s)}(k, \mu = 0)$, and the measured PVD σ_{12} is usually a function of k . Adopting equation (4) for the damping function and setting $\beta = 0.45$, Jing & Börner (2001b) measured the PVD $\sigma_{12}(k)$ for the LCRS and found that the measured PVD is consistent with the result reported by JMB98 from the redshift-space 2PCF measurement.

Both of the methods described above for determining the PVD of galaxies are based on the measurement of galaxy clustering. Previous studies of galaxy clustering in the local Universe have established that it depends on a variety of quantities, including luminosity (e.g. Norberg et al. 2001; Zehavi et al. 2002, 2005), colour (e.g. Zehavi et al. 2002, 2005), morphology (e.g. Zehavi et al. 2002; Goto et al. 2003), and spectral type (e.g. Norberg et al. 2002; Budavári et al. 2003; Madgwick et al. 2003). It is thus expected that there should be some dependence of the galaxy PVD on these physical properties. Using the 2dFGRS and the method based on the redshift-space power spectrum, JB04 presented the first determination of the PVD for galaxies in different luminosity intervals. The analysis leads to a surprising discovery: the relative velocities of the faint galaxies are very high, around 700 km s^{-1} , reaching values similar to those found for the brightest galaxies in the sample. The relative velocities at the intermediate luminosities $M^* - 1$ [M^* is the characteristic luminosity of the Schechter (1976) function] exhibit a well-defined minimum near 400 km s^{-1} . This discovery indicates that faint galaxies, and the brightest ones, are both preferentially in massive haloes of galaxy cluster size, but most M^* galaxies are in galactic scale haloes. Such a luminosity dependence of the PVD is not reproduced by the halo occupation model of Yang, Mo & van den Bosch (2003), although this model reproduces well the luminosity dependence of the clustering.

In this paper, we use the second data release of the SDSS to examine the dependence of the PVD not only on luminosity, but also, for the first time, on other physical properties such as the stellar mass, star formation rate, stellar surface mass density and concentration. These dependences will provide useful clues about how the luminosity dependence of the PVD is produced in the real Universe. As we will see, the high PVD values measured at faint

luminosities can be explained by a population of red galaxies located in rich groups and clusters, which is otherwise subdominant in many other clustering measures such as the 2PCF and measurements of galaxy-galaxy lensing. The results are consistent with the conjecture made by JB04 for this population. In a separate paper (Li et al. 2005, hereafter Paper I), we have measured the 2PCF for the galaxy samples studied in this paper. Taken together, our determinations of the 2PCF and the PVD should be extremely useful for constraining models of galaxy formation.

In the following section, we briefly describe the measurements of the 2PCFs of galaxies that are presented in Paper I. In Section 3, we describe the method and the results for determining the PVD from the redshift power spectrum. We summarize our results in the final section.

Throughout this paper, we assume a cosmological model with the density parameter $\Omega_0 = 0.3$ and the cosmological constant $\Lambda_0 = 0.7$. To avoid the $-5 \log_{10} h$ constant, the Hubble constant $h = 1$, in units of $100 \text{ km s}^{-1} \text{ Mpc}^{-1}$, is assumed throughout this paper when computing absolute magnitudes. In this paper, the quantities with a superscript asterisk are those at the characteristic luminosity/mass (e.g. characteristic luminosity L^*), while the quantities with a subscript asterisk are those of stars (e.g. stellar mass M_*).

2 MEASUREMENTS OF THE TWO-POINT CORRELATION FUNCTIONS

In Paper I, we described in detail our procedure for constructing the observational and random samples and for measuring the 2PCFs in redshift space. The samples analysed here are exactly the same as those presented in Paper I and the reader is referred to this paper for more details.

The redshift-space 2PCF $\xi^{(s)}(r_p, \pi)$ for each subsample is measured using the Hamilton (1993) estimator,

$$\xi^{(s)}(r_p, \pi) = \frac{4DD(r_p, \pi)RR(r_p, \pi)}{[DR(r_p, \pi)]^2} - 1. \quad (5)$$

Here $DD(r_p, \pi)$ is the count of data-data pairs with perpendicular separations in the bins $r_p \pm 0.5\Delta r_p$ and with radial separations in the bins $\pi \pm 0.5\Delta\pi$, $RR(r_p, \pi)$ and $DR(r_p, \pi)$ are similar counts of random-random and data-random pairs, respectively. When computing 2PCFs, some possible biases such as the variance in mass-to-light ratio and fibre collisions have been carefully corrected (see Paper I for a detailed description). Figs 1 and 2 show the contours of $\xi^{(s)}(r_p, \pi)$ for galaxies of different luminosities and of different stellar masses, respectively. Both the effect of redshift-space distortions on small scales (often called the Finger-of-God effect) and the infall effect (Kaiser 1987) on large scales are clearly visible: on small scales $\xi^{(s)}(r_p, \pi)$ is stretched in the π -direction and on large scales the contours are squashed along the line-of-sight direction.

In Paper I, we presented the projected 2PCF $w_p(r_p)$ which is estimated from $\xi^{(s)}(r_p, \pi)$. With this estimator, we investigated the clustering properties of galaxies with various physical properties. In the next section, we will present their real-space power spectra and the PVDs.

3 THE POWER SPECTRUM AND THE PAIRWISE VELOCITY DISPERSION

3.1 Method

Following the method of JB04, we obtain for each subsample the redshift-space power spectrum as

$$P^{(s)}(k, \mu) = 2\pi \sum_{i,j} \Delta\pi_i r_{p,j}^2 \Delta \ln r_{p,j} \xi^{(s)}(r_{p,j}, \pi_i) \cos(k_\pi \pi_i) J_0(k_p r_{p,j}) W_g(r_{p,j}, \pi_i), \quad (6)$$

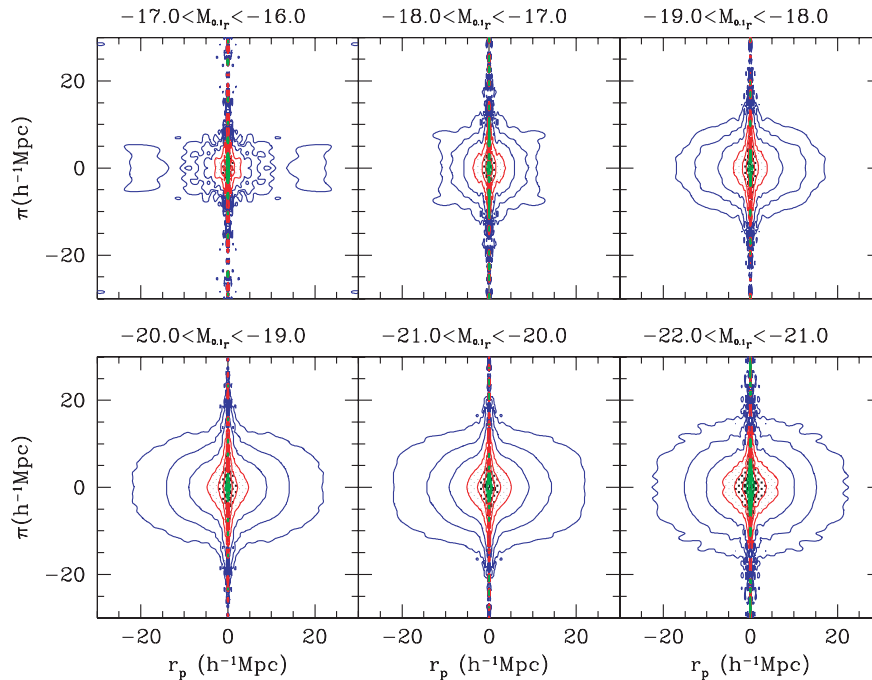


Figure 1. The redshift-space 2PCF $\xi^{(s)}(r_p, \pi)$ in different luminosity intervals, as indicated. The contour levels are increased by factors of 2 from the lowest (0.1875) to the highest (48.0).

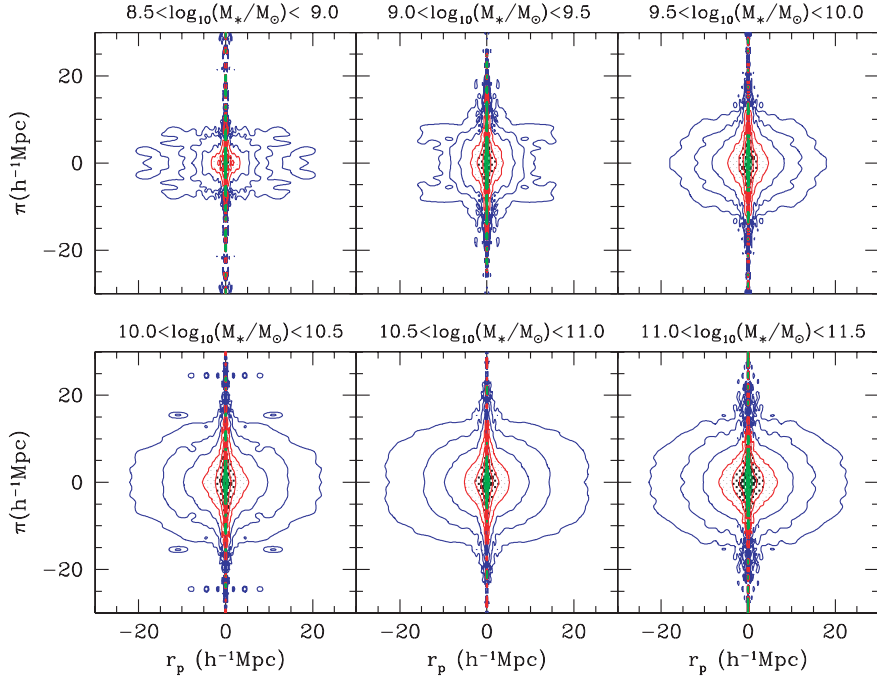


Figure 2. The redshift-space 2PCF $\xi^{(s)}(r_p, \pi)$ in different stellar mass intervals, as indicated. The contour levels are increased by factors of 2 from the lowest (0.1875) to the highest (48.0).

where J_0 is the zeroth-order Bessel function (Jing & Börner 2001b); k_p and k_π are the wavenumbers perpendicular and parallel to the line of sight, and are related to k and μ with

$$k = \sqrt{k_p^2 + k_\pi^2}, \quad \mu = k_\pi/k. \quad (7)$$

Here π_i runs from -40 to $40 h^{-1}$ Mpc with $\Delta \pi_i = 1 h^{-1}$ Mpc and $r_{p,j}$ from 0.1 to $50 h^{-1}$ Mpc with $\Delta \ln r_{p,j} = 0.23$. W_g is the Gaussian window function, which is used to improve the measurement by down weighting $\xi^{(s)}(r_p, \pi)$ at the larger scales and has the form

$$W_g(r_p, \pi) = \exp\left(-\frac{r_p^2 + \pi^2}{2S^2}\right). \quad (8)$$

The smoothing scale is set to be $S = 20 h^{-1}$ Mpc following JB04. With these parameters, JB04 showed that the real-space $P(k)$ and the PVD $\sigma_{12}(k)$ can be reliably measured at scales $k > 0.1 h \text{ Mpc}^{-1}$ and $k > 0.2 h \text{ Mpc}^{-1}$, respectively.

From the measurement of the redshift-space power spectrum $P^{(s)}(k, \mu)$, we can determine the real-space power spectrum $P(k)$ and the PVD σ_{12} simultaneously by modelling the measured $P^{(s)}(k, \mu)$ using equation (3). As discussed in Section 1, it is difficult to simultaneously derive β , σ_{12} and $P(k)$ from $P^{(s)}(k, \mu)$. We therefore fix $\beta = 0.45$ as a reasonable estimate (Tegmark et al. 2004) and determine $P(k)$ and σ_{12} from the data. We will show in the next section that the determinations of the PVD are robust to reasonable changes of the β values.

3.2 The dependence on luminosity

In Fig. 3, the symbols with error bars show the measured power spectrum in redshift-space $P^{(s)}(k, \mu)$. The four panels correspond to four different luminosity intervals (samples L5, L7, L9, and L11, in table 1 of Paper I). In each panel, the values of k range from $0.1 h \text{ Mpc}^{-1}$ at the top, to $4.0 h \text{ Mpc}^{-1}$ at the bottom, with an increment of $\Delta \log_{10} k = 0.2$. The error bars plotted in this figure and in all

subsequent figures are estimated by the bootstrap resampling technique (Barrow, Bhavsar & Sonoda 1984). We generate 100 bootstrap samples and compute the power spectrum for each sample using the weighting scheme (but not the approximate formula) given by Mo, Jing & Börner (1992). The errors are the scatter of the power spectra among these bootstrap samples. The solid lines are the best fits obtained by applying equation (3) to the data. The real-space power spectrum $P(k)$, determined from the modelling with equation (3), is displayed in Fig. 4 for six luminosity samples (Samples L5, L7, L9, L10, L11 and L13, of table 1 in Paper I). To see the systematic change with the luminosity, a function $P(k) = (60/k)^{1.4}$ is plotted as the dashed line in each panel. From both the figures, it is seen that there exists a luminosity dependence of the real-space power spectrum: $P^{(s)}(k, \mu = 0)$ and $P(k)$ increase with increasing luminosity on all scales, with the luminosity dependence becoming stronger for bright galaxies and on small scales. This result is consistent with that in JB04 for the 2dFGRS, and with our analysis of the 2PCF in Paper I. Such a dependence on luminosity was also found for the 2PCF by Norberg et al. (2002) using the 2dFGRS and by Zehavi et al. (2005) using the SDSS. The real-space power spectrum $P(k)$ is approximately a power law for the range of k considered here. The dotted lines in Fig. 4 are the best power-law fits to the measured $P(k)$ with the best-fitting parameters indicated in each panel. $P(k)$ decreases with k approximately as $k^{-1.4}$, with the slopes of the brightest samples being somewhat shallower ($\sim k^{-1.2}$). Moreover, Fig. 4 shows that there is a slight change in the slope of $P(k)$ at $k \approx 1 h \text{ Mpc}^{-1}$ for faint galaxies and at $k \approx 0.5 h \text{ Mpc}^{-1}$ for bright ones. Such a change in slope is much less pronounced in JB04, but it is evident here due to the improvement in the observational data. As pointed out by JB04, such a change can be understood as the transition between the scales where the pair counts are dominated by galaxy pairs in the same halo to those where galaxy pairs are mostly in separate haloes. This result may indicate that fainter galaxies tend to reside in smaller haloes, while brighter galaxies are found

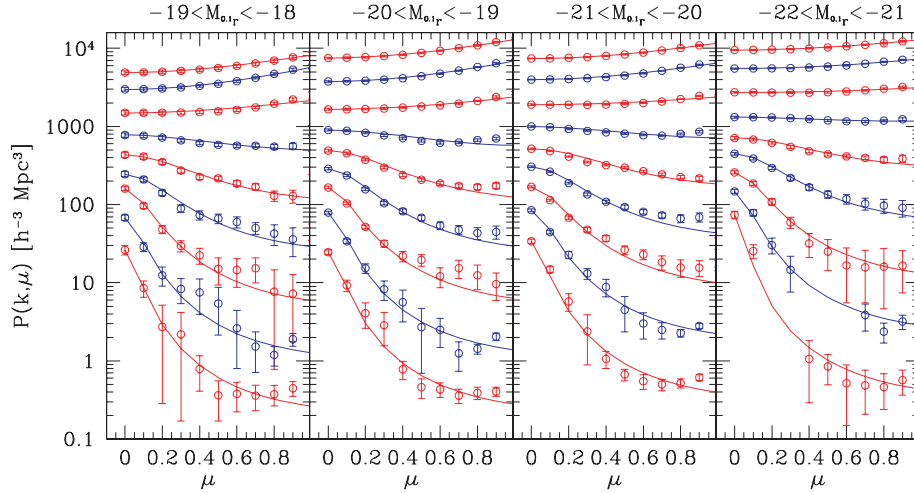


Figure 3. The redshift-space power spectrum $P^{(s)}(k, \mu)$ (symbols with error bars) for galaxies in different luminosity intervals, as indicated above each panel. The lines are the best fits of equation (3) to the data. In each panel, from top to bottom, the wavenumber k is 0.1, 0.16, 0.25, 0.4, 0.63, 1.0, 1.58, 2.51 and $3.98 h \text{ Mpc}^{-1}$, respectively.

in massive haloes, but a more detailed analysis is needed to explain the subtle changes of the power spectrum shape with luminosity. It is interesting to note that such a transition was also found by Zehavi et al. (2004) in the projected 2PCF of galaxies.

Fig. 5 shows the PVD $\sigma_{12}(k)$, which is measured simultaneously with $P(k)$, for galaxies in different luminosity intervals. The errors of $\sigma_{12}(k)$ are also estimated by bootstrap resampling technique. It can be seen that for the k -values used here, $\sigma_{12}(k)$ is a well-determined quantity. As discussed in Section 1, there could be a luminosity dependence of the linear redshift-distortion parameter β , so a fixed value of β might have some impact on our results. We investigate this by using the luminosity dependence of the bias parameter $b(M)/b^* = 0.895 + 0.150(L/L^*) - 0.040(M - M^*)$ given in Tegmark et al. (2004) and $\beta^* = 0.45$ (quantities with an asterisk are defined to be at the characteristic luminosity L^*). The results are plotted in Fig. 5 and agree with those obtained for $\beta = 0.45$ within

the error bars. The largest differences are seen for bright galaxies on very large scales. This indicates that our $\sigma_{12}(k)$ measurements are robust to reasonable changes of the β values.

The dependence of the PVD on luminosity is clearly seen in this figure. The observed PVD for L^* galaxies (the $-21 < M_{0.1r} < -20$ sample) is constant around 500 km s^{-1} at all scales. For faint galaxies, the PVD values increase as a function of k , reach a maximum value of 650 km s^{-1} at $k \simeq 1 h \text{ Mpc}^{-1}$ and then decrease again. For bright galaxies, the behaviour is very different. The PVD values decrease as a function of k , reach a minimum value of 400 km s^{-1} at $k \simeq 0.5 h \text{ Mpc}^{-1}$ and then increase. It is interesting that these main features agree with the findings by JB04 for the 2dFGRS, indicating that the PVD as a function of the scale k and the luminosity are robustly determined with these surveys. As shown by JB04, these features could not be reproduced by the halo model of Yang et al. (2003), because the model predicts that the PVD increases

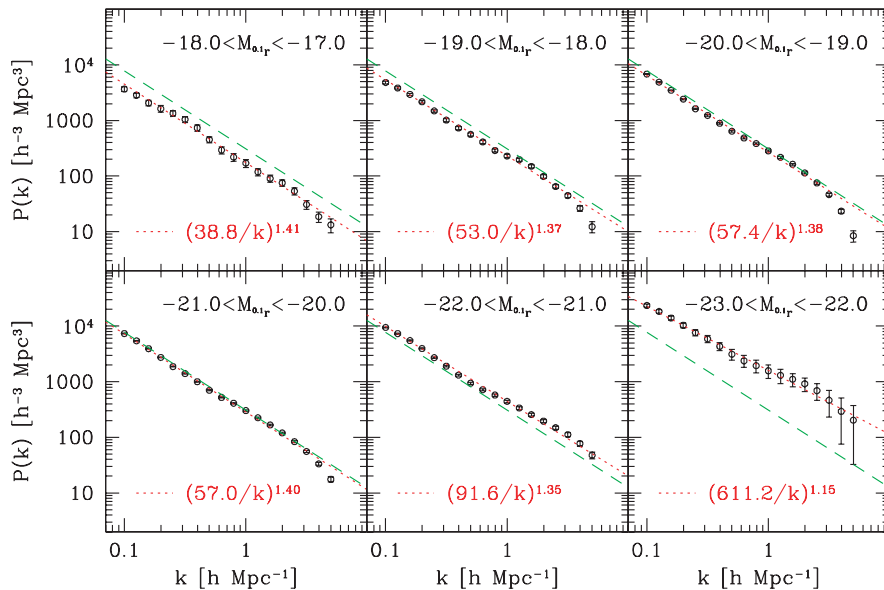


Figure 4. The real-space power spectrum $P(k)$ for galaxies in different luminosity intervals, as indicated. The dotted lines are the power-law fits with the best-fitting parameters indicated in each panel. To guide the eye, the power spectrum $P(k) = (60/k)^{1.4}$ is plotted as dashed line in every panel.

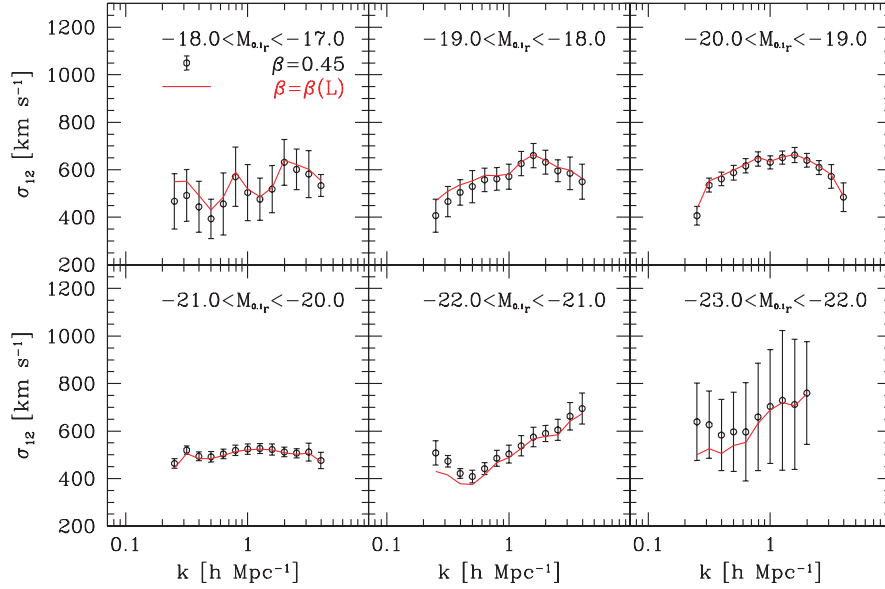


Figure 5. The PVD σ_{12} for galaxies in different luminosity intervals, as indicated. The symbols with errorbars are for the results that are obtained by fixing the redshift-distortion parameter $\beta = 0.45$, while the lines are for those with β varying with luminosity as in Tegmark et al. (2004).

monotonically on small scales. Recently, Slosar, Seljak & Tasitsiomi (2006) made an attempt to interpret the observed luminosity dependence of the PVD in the context of a halo model, and showed that the luminosity dependence of the PVD can be predicted if some of the faint galaxies are the satellite galaxies in high mass haloes, which is consistent with what JB04 expected as well as with the galaxy formation models and the halo occupation distribution (HOD) modelling (e.g. Guzik & Seljak 2002; Berlind et al. 2005; Zehavi et al. 2005). However, a quantitative HOD model that can simultaneously match the observations, such as the luminosity functions, the correlation functions and the PVDs, still needs to be worked out. The observed features of the PVD are very sensitive to how the galaxies of different luminosity are distributed among dark matter haloes and also inside these haloes. The PVD is therefore a good constraint on both the semi-analytical models of galaxy formation and the halo occupation models for the galaxy distribution.

The luminosity dependence of the PVD is shown more clearly in Fig. 6, where we have plotted σ_{12} at $k = 0.25, 0.5, 1$ and $4 h \text{ Mpc}^{-1}$ for galaxies of different luminosities. We again see that the observed PVD for M^* galaxies does not depend on k -value. On large scales ($k = 0.25 h \text{ Mpc}^{-1}$), σ_{12} rises as a function of increasing luminosity. However, on small scales, the PVD exhibits a well-defined minimum at luminosities around $M^* - 1$. The values of σ_{12} at this minimum are $\simeq 500 \text{ km s}^{-1}$ at $k = 1 h \text{ Mpc}^{-1}$ and $\simeq 400 \text{ km s}^{-1}$ at $k = 0.5 h \text{ Mpc}^{-1}$. We thus conclude that bright and faint galaxies have higher random motions than galaxies of the intermediate luminosity. The maximum relative velocities of faint galaxies ($\simeq 600 \text{ km s}^{-1}$) occur on scales $\sim 1 h \text{ Mpc}^{-1}$. For the brightest galaxies, the maximum values occur on the smallest scales and reach values close to 1000 km s^{-1} .

It is interesting to compare the results presented in this paper with those of JB04. To do this, one must transform from the luminosities measured in the b_J band in the 2dFGRS to those measured in the $^{0.1}r$ band in the SDSS. According to the luminosity functions in the two surveys (Madgwick et al. 2002; Blanton et al. 2003), the average difference in absolute magnitude in the two bands is $\sim 0.9 \text{ mag}$. In Fig. 7, we compare our SDSS results with those of

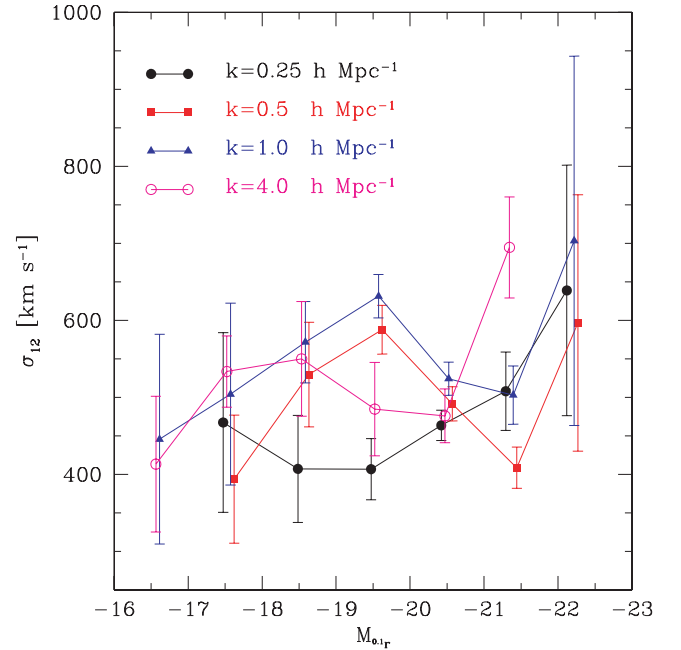


Figure 6. The PVD σ_{12} as a function of luminosity, measured at $k = 0.25, 0.5, 1.0$ and $4.0 h \text{ Mpc}^{-1}$. For clarity, small constants were added to the $M_{0.1r}$ values for the curves of $k = 0.25, 0.5$ and $4.0 h \text{ Mpc}^{-1}$.

the 2dFGRS, after taking into account this difference. It can be seen that the two measurements are quite consistent with each other. It is worth noting that the agreement is almost perfect for luminosities brighter than -19.5 , but for fainter luminosities, σ_{12} is slightly smaller as measured from the SDSS compared to the 2dFGRS. The latter may be due to the fact the volumes covered by the faint samples are not sufficiently large (Mo et al. 1997). The results obtained with varying β are also plotted in this figure. We also plot the prediction for the 2dFGRS PVD of JB04 based on the halo model of

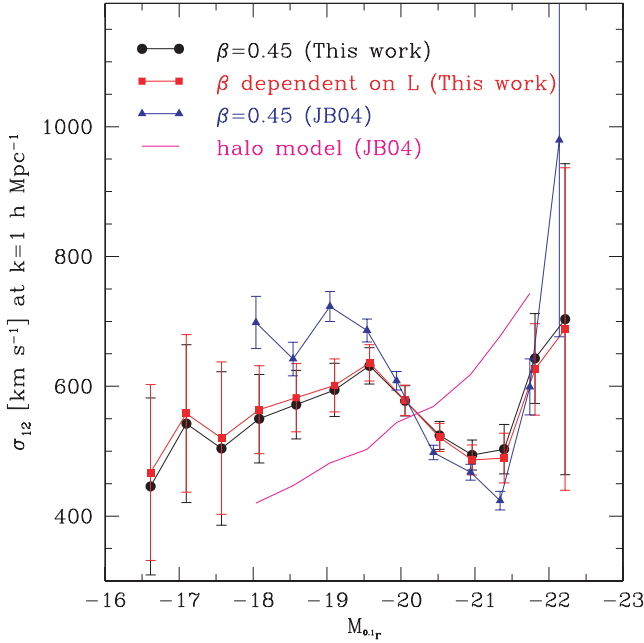


Figure 7. The PVD σ_{12} measured at $k = 1 h \text{ Mpc}^{-1}$ in the SDSS (circles, $\beta = 0.45$; squares, β varies with luminosity as in Tegmark et al. 2004), compared with that in the 2dFGRS (triangles) presented by JB04. The line without symbols shows the prediction of the HOD model of Yang et al. (2003).

Yang et al. (2003), which clearly does not match the observations. The σ_{12} measurements as a function of luminosity are listed in Table 1.

3.3 The dependence on $g - r$, D_{4000} , C and μ_*

To probe the dependence of the PVD on the parameters related to the recent star formation history of galaxies ($g - r$, D_{4000}) and on the parameters related to galaxy structure (C , μ_*), we divide the galaxies into two subclasses: galaxies with larger values of the given physical quantity (hereafter denoted as ‘red’ galaxies) and galaxies

Table 1. The results of the PVD at $k = 1 h \text{ Mpc}^{-1}$ of the luminosity subsamples.

| Sample | Median magnitude $M_{0.1r}$ | $\sigma_v [\beta = 0.45]^a$ (km s^{-1}) | $\sigma_v [\beta(L)]^b$ (km s^{-1}) |
|----------|--------------------------------|---|---|
| L1..... | -16.61 | 446 ± 136 | 467 ± 135 |
| L2..... | -17.10 | 542 ± 122 | 558 ± 121 |
| L3..... | -17.57 | 504 ± 118 | 520 ± 117 |
| L4..... | -18.08 | 550 ± 68 | 564 ± 68 |
| L5..... | -18.58 | 572 ± 53 | 582 ± 53 |
| L6..... | -19.10 | 594 ± 41 | 601 ± 41 |
| L7..... | -19.57 | 631 ± 28 | 636 ± 28 |
| L8..... | -20.06 | 578 ± 23 | 578 ± 23 |
| L9..... | -20.52 | 524 ± 22 | 521 ± 22 |
| L10..... | -20.96 | 494 ± 23 | 487 ± 23 |
| L11..... | -21.39 | 503 ± 38 | 489 ± 38 |
| L12..... | -21.81 | 643 ± 69 | 626 ± 70 |
| L13..... | -22.22 | 703 ± 240 | 688 ± 248 |

^aThe PVD determined with $\beta = 0.45$.

^bThe PVD determined with the luminosity dependence of β taken into account.

with smaller values (hereafter denoted as ‘blue’ galaxies). These subsamples were described in section 2 of Paper I.

Fig. 8 shows the real-space power spectrum $P(k)$ in the space of luminosity versus the physical quantities. The results are compared with the measurements of $w_p(r_p)$ presented in Paper I. As can be seen, the results of $P(k)$ and $w_p(r_p)$ are qualitatively very similar. Galaxies with redder colours, stronger 4000-Å breaks, more concentrated structure and higher surface densities have higher clustering amplitude on all scales and at all luminosities, with the difference more pronounced on small scales and for faint galaxies. Furthermore, the dependence on parameters associated with recent star formation is much stronger than the dependence on structural parameters.

Fig. 9 shows the dependence of the PVD σ_{12} on k for galaxies with different luminosities and physical properties. The samples and the symbols are the same as in Fig. 8. In Fig. 10, we plot σ_{12} measured at $k = 0.25, 0.5, 1$ and $4 h \text{ Mpc}^{-1}$ as a function of luminosity for galaxies with different physical properties. Plots corresponding to Figs 9 and 10, as a function of stellar mass rather than luminosity are shown in Figs 11 and 12. We find that red galaxy populations as defined by both $g - r$ and D_{4000} and early-type galaxy populations as defined by C and μ_* have larger relative velocities on all scales and at all luminosities/masses than blue and late-type populations. We can also see that the dependence of σ_{12} on these physical properties is stronger for faint/low-mass galaxies and on small scales. On very large scales, galaxies of all luminosities/masses have very similar pairwise peculiar velocities.

In order to study the detailed dependence of the PVD on galaxy properties, we restrict our analysis to galaxies with stellar masses in the range $10 < \log_{10} M_* < 11$, and divide the sample into subsamples with finer bins in $g - r$, D_{4000} , C and μ_* (see table 3 of Paper I). In Fig. 13, we show the PVD σ_{12} on different scales, as a function of these quantities. The dependences of σ_{12} on quantities related to past star formation history and on quantities related to galaxy structure are quite different. Fig. 13 shows that σ_{12} increases with increasing $g - r$ or D_{4000} . On the other hand, σ_{12} as a function of concentration exhibits a maximum at $C \sim 2.6$ for $k = 0.25 h \text{ Mpc}^{-1}$ and at $C \sim 2.8$ for larger k values, reaching $\sim 700 \text{ km s}^{-1}$ on small scales and $\sim 500 \text{ km s}^{-1}$ on large scales. Furthermore, on very small scales, ‘star-forming’ galaxies with $D_{4000} < 1.5$ have nearly constant peculiar velocities ($\sim 300 \text{ km s}^{-1}$), while σ_{12} increases sharply above $D_{4000} = 1.5$, reaching $\sim 1000 \text{ km s}^{-1}$ for galaxies with $D_{4000} = 2$. The PVD is an indicator of the depth of the local gravitational potential. Therefore, we are led to the conclusion that the reddest galaxies move in the strongest gravitational fields. A substantial fraction of these red galaxies must reside in clusters, while most galaxies with blue colours, recent star formation, and diffuse structure populate the field. Interestingly, the behaviour of σ_{12} as a function of concentration is more complicated. Galaxies with the *intermediate* value of C have the highest relative velocities. This may indicate that many red galaxies in clusters are really spirals whose ongoing star formation has been truncated.

4 DISCUSSION AND CONCLUSIONS

In this paper, we have made a detailed study of the power spectrum and the PVDs of galaxies classified according to their luminosity, stellar mass, colour, 4000-Å break, concentration index, and stellar surface mass density, using the SDSS DR2. Our results can be summarized as follows:

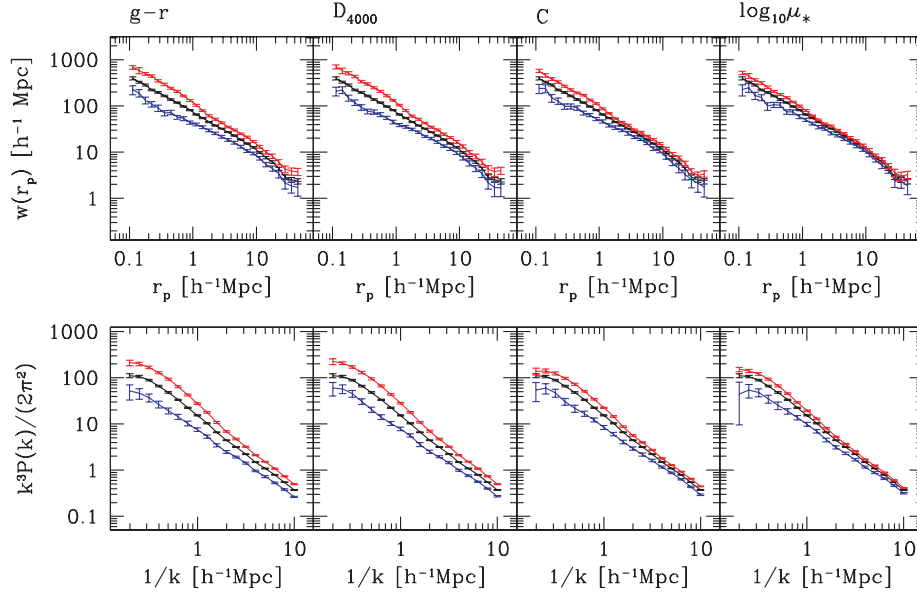


Figure 8. The real-space power spectrum $P(k)$ [the bottom panels; here the power spectra are given in the power-per-log-interval presentation: $\Delta^2(k) = k^3 P(k)/(2\pi^2)$] for galaxies in the luminosity interval of $-21 < M_{0.1r} < -20$ and with different properties (from the left-hand to right-hand panel: $g-r$ colour, D_{4000} , concentration and $\log_{10} \mu_*$), compared to the corresponding $w_p(r_p)$ measurements (top panels) from Paper I (see the third row in fig. 10 of Paper I). In each panel, the black is for the full sample, while the red (blue) is for the subsample with larger (smaller) value of the corresponding physical parameter.

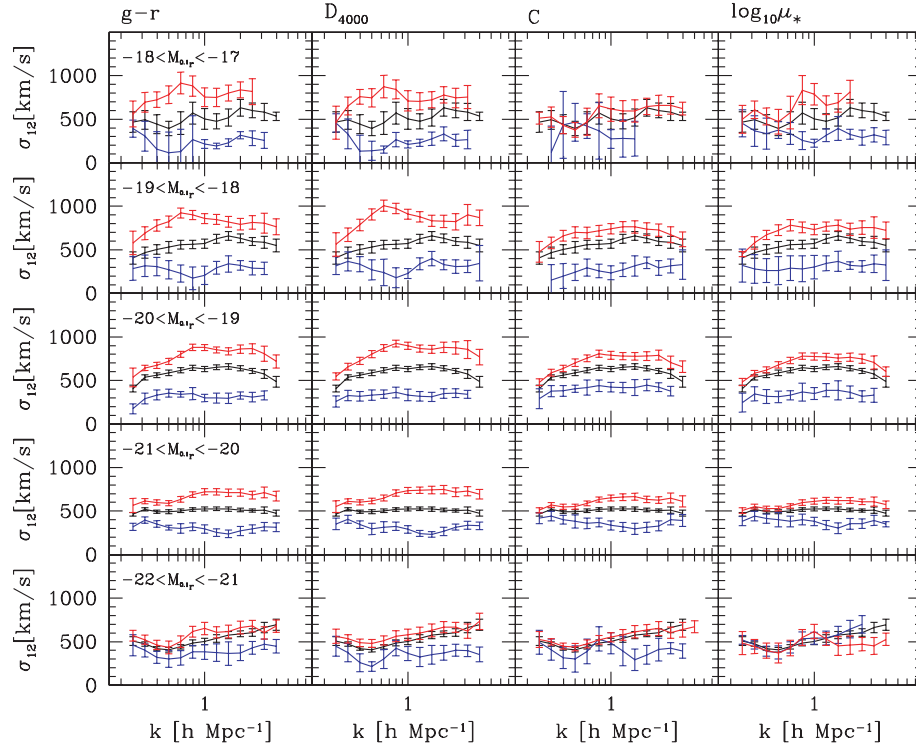


Figure 9. The PVD σ_{12} for galaxies with various luminosities and physical properties. Panels from the top to bottom panel correspond to galaxies in different luminosity intervals (as indicated in the first column), while panels from the left-hand to right-hand panel correspond to galaxies divided by different physical quantities (as indicated above each column). In each panel, red (blue) is for the subsample with larger (smaller) value of the corresponding physical quantity, while black is for the full sample.

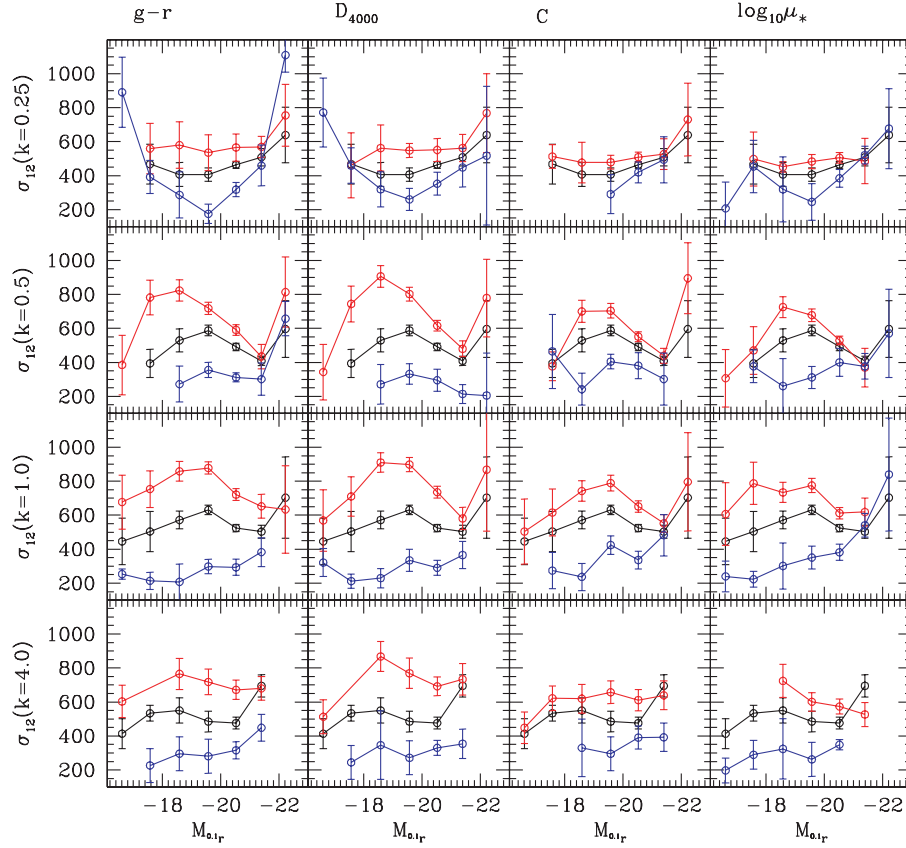


Figure 10. The PVD $\sigma_{12}(k)$ as a function of absolute magnitude, measured at $k = 0.25, 0.5, 1$ and 4 h Mpc^{-1} for different classes of galaxies. Panels from the top to bottom panel correspond to measurements on different wavenumbers, while panels from the left-hand to right-hand panel correspond to galaxies divided by different physical quantities, as indicated above each column. In each panel, red (blue) is for the subsample with larger (smaller) value of the corresponding physical quantity, while black is for the full sample.

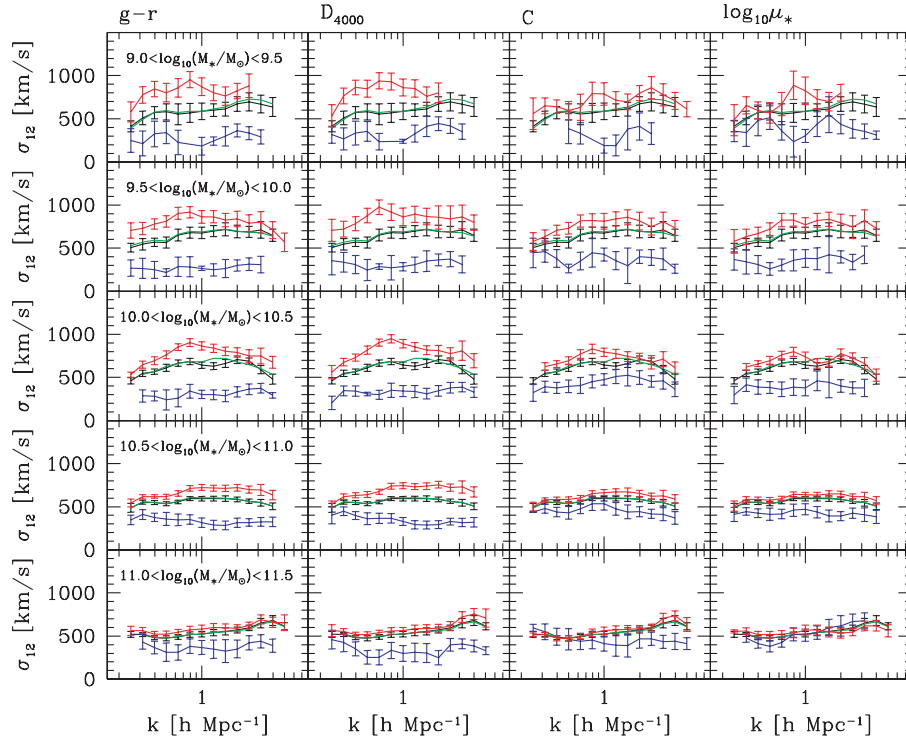


Figure 11. The PVD σ_{12} for galaxies with various stellar masses and physical properties. The symbols are the same as in Fig. 9, except that the green line in each panel is for the full sample volume-limited in stellar mass.

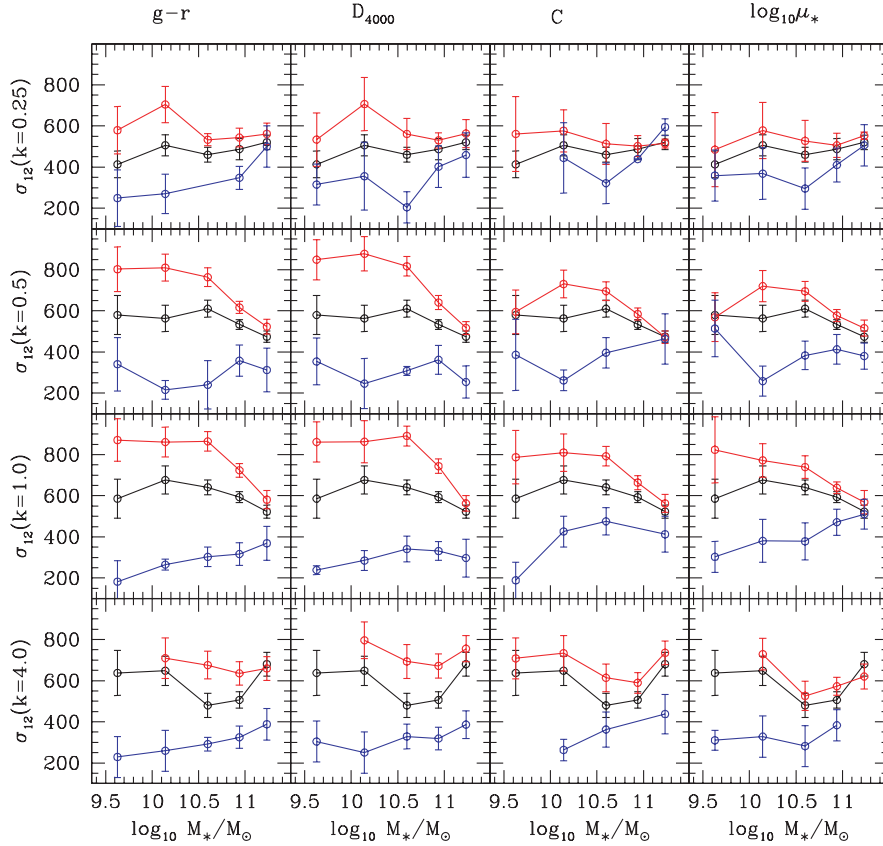


Figure 12. The PVD $\sigma_{12}(k)$ as a function of stellar mass, measured at $k = 0.25, 0.5, 1$ and $4 h \text{ Mpc}^{-1}$ for different classes of galaxies. The symbols are the same as in Fig. 10.

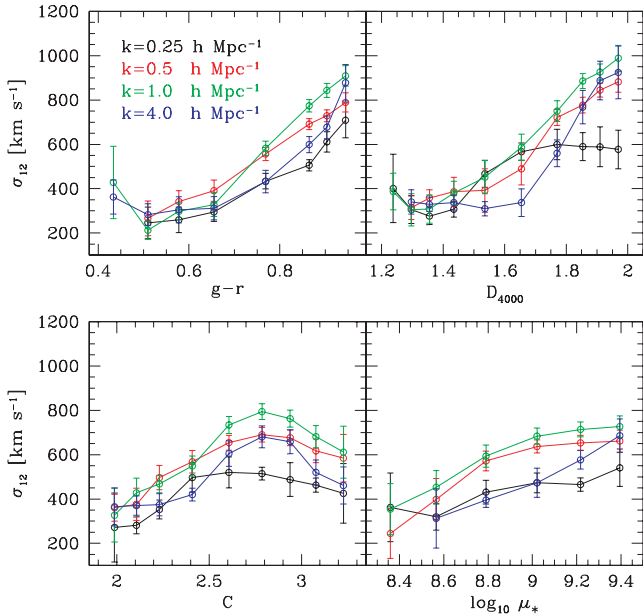


Figure 13. The PVD σ_{12} as a function of various physical quantities, measured at $k = 0.25, 0.5, 1$ and $4 h \text{ Mpc}^{-1}$ (as indicated in the top-left panel). All the samples are selected to lie in the stellar mass range $10 < \log_{10} M_* < 11$.

(i) The real-space power spectrum and the PVD as a function of luminosity in the SDSS are in good agreement with the result presented by Jing & Börner (2004) for the 2dFGRS, after taking into account the photometric bandpass difference between the two surveys.

(ii) Galaxies with redder colours, stronger 4000-Å breaks, more concentrated structure and higher surface mass densities have larger clustering power and larger relative velocities on all scales and at all luminosities/stellar masses.

(iii) The dependences of the clustering power and PVD on the parameters related to recent star formation are stronger than those on the parameters related to galaxy structure, especially on small scales and for faint galaxies.

(iv) The reddest galaxies and galaxies of the intermediate concentrations move in the deepest gravitational field. A large fraction of these objects must reside in clusters, while most galaxies with blue colours, recent star formation, and diffuse structure populate the field.

From the above results, it is not difficult to understand why the PVD on small scales ($k = 1 h \text{ Mpc}^{-1}$) exhibits a minimum at $M^* - 1$, and why faint galaxies have larger relative velocities than bright galaxies (JB04). As seen both in Fig. 8 in this paper and in fig. 10 of Paper I, faint red galaxies are more strongly clustered than faint blue galaxies, and have comparable or even greater clustering power than bright red galaxies. However, the majority of faint galaxies have blue colours and cluster weakly. The fraction of red galaxies is only about 30 per cent for luminosities fainter than -19 (table 1 of Paper I). This means that the power spectrum of faint galaxies is dominated by the blue population, which leads to a monotonic

increase of the clustering strength with luminosity (Norberg et al. 2001; Tegmark et al. 2004; Zehavi et al. 2005). However, the faint red population in rich clusters, even though small in number, can dominate the PVD on small scales, because the PVD is more sensitive to the galaxy population in rich clusters than the power spectrum (see Mo et al. 1997, for a discussion). This is also clearly seen in Fig. 10. Our results therefore support the conjecture made by JB04 that a large fraction of the faint galaxy population must reside in rich clusters. We demonstrate that this fraction is predominantly red.

Although most of the results presented in this paper can be understood qualitatively by considering known trends in galaxy properties as a function of environment, a quantitative understanding requires galaxy formation models (e.g. Kauffmann, White & Guiderdoni 1993; Cole et al. 1994; Kauffmann, Nusser & Steinmetz 1997; Kauffmann et al. 1999; Somerville & Primack 1999; Cole et al. 2000; Croton et al. 2006; Kang et al. 2005) or halo occupation models (e.g. Jing et al. 1998; Seljak 2000; Berlind & Weinberg 2002; Cooray & Sheth 2002; Yang et al. 2003; Zheng 2004; Slosar et al. 2006). Through such studies, the results in this paper will provide stringent constraints on these models, and will provide important clues where galaxies of different physical properties are located and how they have formed and evolved.

ACKNOWLEDGMENTS

We are grateful to Dr Michael Blanton for his help with the NYU-VAGC. We thank the SDSS teams for making their data publicly available and the referee for a detailed report. This work is supported by NKBRSF(G19990754), by NSFC(Nos.10125314, 10373012, 10073009), by Shanghai Key Projects in Basic research (04jc14079, 05xd14019), by the Max Planck Society, and partly by the Excellent Young Teachers Programme of MOE, P.R.C. CL acknowledges the financial support of the exchange programme between Chinese Academy of Sciences and the Max Planck Society.

Funding for the creation and distribution of the SDSS Archive has been provided by the Alfred P. Sloan Foundation, the Participating Institutions, the National Aeronautics and Space Administration, the National Science Foundation, the U.S. Department of Energy, the Japanese Monbukagakusho, and the Max Planck Society. The SDSS website is <http://www.sdss.org/>.

The SDSS is managed by the Astrophysical Research Consortium (ARC) for the Participating Institutions. The Participating Institutions are The University of Chicago, Fermilab, the Institute for Advanced Study, the Japan Participation Group, The Johns Hopkins University, Los Alamos National Laboratory, the Max-Planck-Institute for Astronomy (MPIA), the Max-Planck-Institute for Astrophysics (MPA), New Mexico State University, Princeton University, the United States Naval Observatory, and the University of Washington.

REFERENCES

Barrow J. D., Bhavsar S. P., Sonoda D. H., 1984, *MNRAS*, 210, 19
Berlind A. A., Weinberg D. H., 2002, *ApJ*, 575, 587

Berlind A. A., Blanton M. R., Hogg D. W., Weinberg D. H., Davé R., Eisenstein D. J., Katz N., 2005, *ApJ*, 629, 625
Blanton M. R., Lin H., Lupton R. H., Maley F. M., Young N., Zehavi I., Loveday J., 2003, *ApJ*, 592, 819
Budavári T. et al., 2003, *ApJ*, 595, 59
Cole S., Aragon-Salamanca A., Frenk C. S., Navarro J. F., Zepf S. E., 1994, *MNRAS*, 271, 781
Cole S., Fisher K. B., Weinberg D. H., 1995, *MNRAS*, 275, 515
Cole S., Lacey C. G., Baugh C. M., Frenk C. S., 2000, *MNRAS*, 319, 168
Cooray A., Sheth R., 2002, *PhR*, 372, 1
Croton D. J. et al., 2006, *MNRAS*, 365, 11
Davis M., Peebles P. J. E., 1983, *ApJ*, 267, 465
Davis M., Efstathiou G., Frenk C. S., White S. D. M., 1985, *ApJ*, 292, 371
Diaferio A., Geller M. J., 1996, *ApJ*, 467, 19
Fisher K. B., Davis M., Strauss M. A., Yahil A., Huchra J. P., 1994b, *MNRAS*, 267, 927
Goto T., Yamaguchi C., Fujita Y., Okamura S., Sekiguchi M., Smail I., Bernardi M., Gomez P., 2003, *MNRAS*, 346, 601
Guzik J., Seljak U., 2002, *MNRAS*, 335, 311
Hamilton A. J. S., 1993, *ApJ*, 417, 19
Hawkins et al., 2003, *MNRAS*, 346, 78
Jing Y. P., Börner G., 2001a, *ApJ*, 547, 545
Jing Y. P., Börner G., 2001b, *MNRAS*, 325, 1389
Jing Y. P., Börner G., 2004, *ApJ*, 617, 782 (JB04)
Jing Y. P., Mo H. J., Börner G., 1998, *ApJ*, 494, 1 (JMB98)
Kaiser N., 1987, *MNRAS*, 227, 1
Kang X., Jing Y. P., Mo H. J., Börner G., 2005, *ApJ*, 631, 21
Kauffmann G., White S. D. M., Guiderdoni B., 1993, *MNRAS*, 264, 201
Kauffmann G., Nusser A., Steinmetz M., 1997, *MNRAS*, 286, 795
Kauffmann G., Colberg J. M., Diaferio A., White S. D. M., 1999, *MNRAS*, 303, 188
Li C., Kauffmann G., Jing Y. P., White S. D. M., Börner G., Cheng F. Z., 2006, *MNRAS*, this issue (doi: 10.1111/j.1365-2966.2006.10066.x) (Paper I)
Madgwick D. S. et al., 2002, *MNRAS*, 333, 133
Madgwick D. S. et al., 2003, *MNRAS*, 344, 847
Marzke R. O., Geller M. J., da Costa L. N., Huchra J. P., 1995, *AJ*, 110, 477
Mo H. J., Jing Y. P., Börner G., 1992, *ApJ*, 392, 452
Mo H. J., Jing Y. P., Börner G., 1993, *MNRAS*, 264, 825
Mo H. J., Jing Y. P., Börner G., 1997, *MNRAS*, 286, 979
Norberg P. et al., 2001, *MNRAS*, 328, 64
Norberg P. et al., 2002, *MNRAS*, 332, 827
Peacock J. A., Dodds S. J., 1994, *MNRAS*, 267, 1020
Peacock J. A. et al., 2001, *Nat*, 410, 169
Schechter P., 1976, *ApJ*, 203, 297
Scoccimarro R., 2004, *PhRvD*, 70, 083007
Sheth R. K., 1996, *MNRAS*, 279, 1310
Seljak U., 2000, *MNRAS*, 318, 203
Slosar A., Seljak U., Tasitsiomi A., 2006, *MNRAS*, 366, 1455
Somerville R. S., Davis M., Primack J. R., 1997, *ApJ*, 479, 616
Somerville R. S., Primack J. R., 1999, *MNRAS*, 310, 1087
Tegmark M. et al., 2004, *ApJ*, 606, 702
Yang X., Mo H. J., van den Bosch F. C., 2003, *MNRAS*, 339, 1057
Zehavi I. et al., 2002, *ApJ*, 571, 172
Zehavi I. et al., 2004, *ApJ*, 608, 16
Zehavi I. et al., 2005, *ApJ*, 630, 1
Zheng Z., 2004, *ApJ*, 610, 61
Zurek W., Quinn P. J., Salmon T. K., Warren M. S., 1994, *ApJ*, 431, 559

This paper has been typeset from a $\text{\TeX}/\text{\LaTeX}$ file prepared by the author.